Phase Control in Interpolation for Backprojection of THz FMCW SAR Signals

Yevhen Ivanenko[(1)], Viet T. Vu[(1)], Jan Barowski[(2)], Hans Hellsten[(3)], and Mats I. Pettersson[(1)]
[(1)]*Department of Mathematics and Natural Sciences, Blekinge Institute of Technology, 37179 Karlskrona, Sweden*
{yevhen.ivanenko,viet.thuy.vu,mats.pettersson}@bth.se
[(2)]*Department of Electrical Engineering and Information Technologies, Ruhr University Bochum, 44801 Bochum, Germany*
jan.barowski@rub.de
[(3)]*School of Information Technology, Halmstad University, 30118 Halmstad, Sweden*
hans.hellsten@hh.se

***Abstract*—The THz frequency spectrum opens a lot of applications in the imaging at sub-mm level. The increase of the operating frequency band for SAR imaging systems to the THz range has proportionally affected the amount of raw data to be stored and used for accurate image reconstruction. As a consequence, improvements in the existing SAR imaging algorithms to reduce the amount of data needed to achieve the appropriate quality of imaging is desired. This paper introduces the phase control procedure as an extension to the existing sinc interpolator for backprojecting complex-valued FMCW SAR data into a defined image plane. The proposed extension controls the phase of interpolated complex-valued SAR data parameters so that it includes appropriate information about the range distance between the SAR system and the given point of space. The extended algorithm is incorporated into the global backprojection algorithm and examined on the measurement data acquired via the 2πSENSE FMCW SAR system. The efficiency of the extended algorithm is evaluated through the comparison with the conventional nearest neighbor and sinc interpolation algorithms.**

***Index Terms*—SAR data interpolation, FMCW Backprojection, FMCW SAR, THz.**

I. Introduction

Synthetic aperture radar (SAR) is the radar system mounted on a moving platform, such as a satellite, aircraft, or unmanned aerial vehicle, and has the aperture synthesized based on the path of motion of its platform. The advantage of the synthetic aperture is that its size can be much larger than the physical aperture of the radar antenna, which provides an opportunity to perform high-resolution imaging in the cross-range direction. Among the wide range of SAR applications, including change detection and ground moving target identification, the most fundamental application of SAR is radar imaging. SAR imaging can be performed at distances starting from hundreds of kilometers from the Earth's surface to below one meter for short-range sensing [1]. Large-distance imaging can be used to study geology, and indoor short-range sensing can be used in the areas of logistics and security, for which the THz-frequency spectrum has to be explored. THz SAR imaging is a very new and active research topic, where the objective is to design an imaging system that can be mounted on various platforms with potential applications in the areas, such as security, logistics, and indoor localization. Most of the state-of-the-art THz SAR systems include ground- and rail-based realizations. Different THz SAR testbeds have been developed to perform imaging at $0.3\,\mathrm{THz}$ [2]–[4], $0.6\,\mathrm{THz}$ [5], $0.75\,\mathrm{THz}$ [6], and up to $1.1\,\mathrm{THz}$, which has been reported recently in [7]. Furthermore, THz SAR systems are realized based on frequency modulated continuous wave (FMCW) radars that operate in the frequency ranges $[0.122; 0.17]\,\mathrm{THz}$ and $[0.126; 0.182]\,\mathrm{THz}$; see [8] and [9], respectively.

However, in practice, the performance of THz SAR imaging systems is sensitive to the path deviation, as reported in [10], [11]. To handle this issue, the time-domain backprojection algorithms [12]–[14] can be used for image formation. These signal processing algorithms can handle signals with large fractional bandwidth and include the motion-compensation procedure [15], which makes them natural candidates to be used in THz SAR imaging systems. The major computational part of these algorithms is based on the interpolation procedure, at which the interpolated complex-valued SAR parameter is backprojected into a defined image plane. There exist various interpolation algorithms that are in SAR data processing. For example, nearest neighbor, piecewise linear, four- and six-point cubic convolution, and truncated sinc interpolators can be used in SAR interferometry, as reported in [16]. Here, six-point cubic convolution interpolator is recommended as optimal for high-resolution applications. The truncated sinc interpolator can be equipped with the Hanning window to improve coherency in SAR interferometry [17]. Recently, extended versions of linear and cubic interpolators with a phase control procedure that assigns information about the range distance between the SAR platform and the given point in space into the phase of interpolated complex-valued parameters have been introduced in [18] to process complex-valued SAR data for pulse radars. The results demonstrate that the proposed procedure provides an opportunity to obtain accurate imaging results with linear and cubic interpolators at the sampling rate $f_\mathrm{s} = 2f_\mathrm{max}$. However, to the knowledge of the authors, none of the existing interpolation algorithms for THz FMCW SAR systems controls information about the phase of estimated complex-valued parameters.

This work was supported by the ELLIIT research environment under the project Multistatic High-resolution Sensing at THz, Project-ID A17.

This paper introduces an extended version of sinc interpolation algorithm that includes the phase control procedure. The proposed procedure is developed to ensure that the phase of interpolated complex-valued FMCW SAR data includes the range distance information between the SAR platform and the point of space in the defined image plane. The developed algorithm is compared with the conventional nearest neighbor and sinc interpolators. All the interpolation algorithms are incorporated into the global backprojection algorithm and tested on raw data acquired via FMCW SAR operating at THz frequencies to reconstruct SAR scenes. Furthermore, the comparison is based on the analysis of range and azimuthal SAR scene cuts, including the measurements of range and cross-range resolutions.

The rest of the paper is organized as follows. Section II describes the basic principles of FMCW SAR, the image formation algorithm, and the supporting interpolation methods. The measurement setup and experimental results are presented in Section III. Finally, the paper is concluded in Section IV.

II. Theory

A. FMCW Synthetic Aperture Radars

Consider a monostatic stripmap FMCW SAR system that performs two-dimensional imaging. Suppose that the FMCW radar transmits a complex-valued linear frequency-modulated continuous-wave signal, which mathematically can be expressed as

$$S_{\mathrm{TX}}(f(t)) = \mathrm{e}^{-\mathrm{j}2\pi(f_{\min}t+\kappa t^2/2)}, \qquad 0 \le t \le T. \quad (1)$$

Here, $f_{\min}$ denotes the start frequency of the emitted frequency ramp, t the range time, and κ and T are the slope and the duration of the emitted frequency ramp, respectively.

Suppose that a scatterer is located in the scene under illumination at the range distance R. The received signal reflected from the target can be written in the simplified form as

$$S_{\mathrm{RX}}(\xi, f(t)) = \mathrm{e}^{-\mathrm{j}2\pi[f_{\min}(t-\tau)+\kappa(t-\tau)^2/2]}. \quad (2)$$

Here, $\tau = 2R/\mathrm{c}_0$ is the range-time delay, where c_0 denotes the speed of light in vacuum and the range distance R can be determined as

$$R = \sqrt{(\xi-\xi')^2 + (\rho-\rho')^2}, \quad (3)$$

where (ξ, ρ) and (ξ', ρ') are azimuthal and range coordinates of the SAR platform antenna and the corresponding target, respectively.

To ensure that the received signal is sampled properly, it is downconverted to the intermediate frequency (IF) domain by performing the mixing of transmitted (1) and received (2) signals as:

$$\begin{aligned} S_{\mathrm{IF}}(\xi, f(t)) &= S_{\mathrm{TX}}(f(t)) S^*_{\mathrm{RX}}(f(t)) \\ &= \mathrm{e}^{-\mathrm{j}2\pi(f(t)\tau-\kappa\tau^2/2)} \approx \mathrm{e}^{-\mathrm{j}2\pi f(t)\tau}. \end{aligned} \quad (4)$$

Here $f(t) = f_{\min} + \kappa t$ so that $f_{\min} \le f(t) \le f_{\max}$ for $t \in [0, T]$, and the second term under the exponential argument in (4) can be neglected for short distances between the aperture antenna and the target at which $f(t)\tau \gg \kappa\tau^2/2$.

Considering the IF signal (4) as a function of frequency f, the time-domain representation of the downconverted signal can be obtained via the inverse Fourier transform as

$$\begin{aligned} s_{\mathrm{IF}}(\xi, t) &= \mathcal{F}^{-1}\{S_{\mathrm{IF}}(\xi, f)\} \\ &= B\,\mathrm{sinc}[\pi B(t-\tau)]\mathrm{e}^{\mathrm{j}2\pi f_{\mathrm{c}}(t-\tau)}, \end{aligned} \quad (5)$$

which is equivalent to the representation of range-compressed signal due to a point target. Here, $B = f_{\max} - f_{\min}$ is the bandwidth, and $f_{\mathrm{c}} = (f_{\max} + f_{\min})/2$ the center frequency. In the presence of multiple targets in the scene under illumination, the downconverted signal in the time domain for this case is considered as a generalization of (5) and can be analytically be expressed via the Born's approximation as

$$g(\xi, t) \approx \sum_{j=1}^{K} B\,\mathrm{sinc}[\pi B(t-\tau_j)]\mathrm{e}^{\mathrm{j}2\pi f_{\mathrm{c}}(t-\tau_j)}, \quad (6)$$

where τ_j, $j = 1, \ldots, K$, denotes the round time needed for a signal to be transmitted from the FMCW SAR aperture antenna to the corresponding j-th target and backwards, and $K \ge 1$, $K \in \mathbb{Z}$, is the total number of targets.

B. Image formation

To form an image based on the acquired IF data, we employ time-domain backprojection in this study. Let the global backprojection algorithm be the algorithm to be used to reconstruct SAR scenes. The algorithm is based on the superposition of received signals that are backprojected into a defined image plane, which can be expressed as

$$h(\xi, \rho) = \int_{-D_{\mathrm{SAR}}/2}^{D_{\mathrm{SAR}}/2} g(\xi, t)\,\mathrm{d}\xi, \quad (7)$$

where D_{SAR} is the length of synthetic aperture, and $g(\xi, t)$ is the range-compressed signal estimated for the given azimuthal position of the FMCW SAR system and the two-range distance between the platform and the point in the defined image plane, which is related to the range time t.

However, modern radar systems, including FMCW radars, operate with discrete signals. The downconverted signal in (4) is discretized with the sampling rate f_{s}, so that the length of the sample sequence can be obtained as $N = f_{\mathrm{s}}T$. Consequently, the frequency variable can be expressed as

$$f[n] = f_{\min} + \frac{\kappa n}{f_{\mathrm{s}}} \quad (8)$$

for $n \in [0, N-1]$. The azimuthal parameter ξ can also be discretized assuming that the FMCW SAR system performs a finite number of measurements M that are equidistantly distributed along the azimuthal axis. The backprojection algorithms for image reconstruction based on the discrete time sequences can then be expressed as

$$h(\xi, \rho) = \sum_{m=1}^{M} g_{\mathrm{int}}[m, t_{\mathrm{p}}], \quad (9)$$

where $m = 1, \ldots, M$ denotes the number of corresponding aperture positions and t_p is the time for signal's trip from SAR antenna aperture to the point of space in the defined image plane. Here, g_int denotes the interpolated complex-valued parameter, which is estimated based on time-domain range compressed data samples

$$g[m,n] = N\,\mathrm{IFFT}\{S_\mathrm{IF}[m,n]\}\mathrm{e}^{\mathrm{j}2\pi f_\mathrm{min} t[n]}, \tag{10}$$

where the phase correction term depends on the frequency f_min at $t = 0$. In this paper, we consider three interpolation algorithms for estimating complex-valued $g_\mathrm{int}[m, t_\mathrm{p}]$.

1) Nearest neighbor (NN) interpolator is one of the conventional and simplest interpolation techniques that estimates the unknown parameter $g_\mathrm{int,NN}$ at t_p through the assigning the data value of one of the two neighbor samples $t[n]$ and $t[n+1]$, $t[n] < t_\mathrm{p} < t[n+1]$. Mathematically, it can be expressed as

$$g_\mathrm{int,NN}[m, t_\mathrm{p}] = \begin{cases} g[m,n], & t[n] \le t_\mathrm{p} < \frac{1}{2}(t[n] + t[n+1]), \\ g[m,n+1], & \frac{1}{2}(t[n] + t[n+1]) < t_\mathrm{p} \le t[n+1]. \end{cases} \tag{11}$$

2) The sinc interpolator is used for ideal reconstruction of bandlimited discrete signals [19]. One of the practical realizations of sinc interpolator is given by

$$g_\mathrm{int,sinc}[m, t_\mathrm{p}] = \sum_{i=n-L}^{n+L} g[m,i] w[i]\,\mathrm{sinc}\left[\frac{\pi(t_\mathrm{p} - t[i])}{T}\right], \tag{12}$$

where the infinite series is truncated up to $2L+1$ terms, $L \ge 0$, $L \in \mathbb{Z}$, and weighted with the Hanning window $w[i]$ to suppress the Gibbs phenomenon. However, the conventional sinc interpolation algorithm does not account for the range distance between the SAR platform and the spatial point in the defined image plane $R_\mathrm{p} = \mathrm{c}_0 t_\mathrm{p}/2$. As a result, the phase of the interpolated complex-valued parameter $g_\mathrm{int,sinc}$ does not contain a correct information about the range time t_p, which requires an extension of the existing interpolation algorithm.

3) The sinc interpolation with the phase control procedure is developed to interpolate complex-valued FMCW SAR data, so that it is ensured that information about the range distance between the SAR platform and the given point of space in the defined image plane is assigned into the phase of the interpolated complex-valued SAR data parameter. The extended sinc interpolator is based on the approach introduced for pulse radars in [18] and mathematically can be expressed as

$$g_\mathrm{int,sincPC}[m, t_\mathrm{p}] = \sum_{i=n-L}^{n+L} \tilde{g}[m,i] w[i]\,\mathrm{sinc}\left[\frac{\pi(t_\mathrm{p} - t[i])}{T}\right], \tag{13}$$

where

$$\tilde{g}[m,i] = g[m,i]\mathrm{e}^{\mathrm{j}2\pi f_\mathrm{c}(t_\mathrm{p} - t[i])}. \tag{14}$$

Here, $\tilde{g}[m,i]$ denotes the data samples involved in the interpolation procedure, the phase of which contains similar information about the assigned range time t_p. The proposed extension increases the complexity of the sinc interpolation algorithm by additional $7(2L+1)$ operations. However, the order of computational complexity of the global backprojection algorithm remains the same $\mathcal{O}\{N_\xi M_\rho M_\xi\}$, where N_ξ is the total number of aperture positions, and M_ξ and M_ρ are the numbers of SAR scene pixels in azimuthal and range directions, respectively.

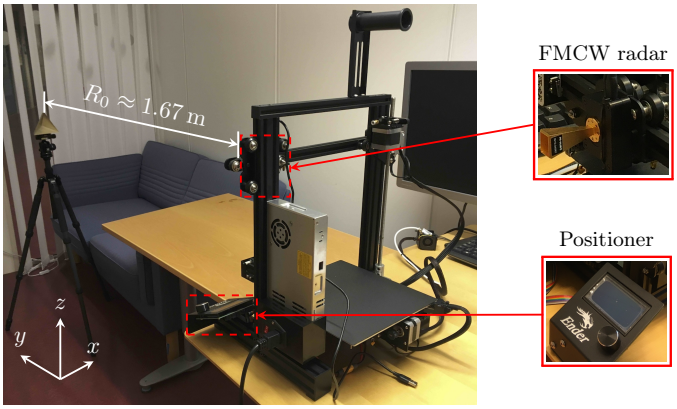

Fig. 1. Measurement setup.

III. Experimentation

In this section, the interpolation algorithms described in Section II-B are tested on FMCW radar signals. The efficiency of the proposed interpolation scheme based on the sinc interpolator is compared with the results based on the nearest neighbor and conventional sinc interpolators. The sinc interpolators used in this section are truncated to $2L+1 = 25$ sinc functions, where $L = 12$. The radar signals were acquired via the 2πSENSE FMCW radar system that operates in the D-frequency band, i.e., in the range $[0.126, 0.182]$ THz.

A. Measurement Setup

The measurement monostatic THz SAR system was based on the D-band 2πSENSE FMCW radar. The radar was mounted on the moving track of the print head of a 3D printer; see Fig. 1. The 3D printer served as a platform for the THz SAR imaging system, for which the maximally achievable aperture length is about 23 cm, and provided spatial system movement with precise accuracy. In the considered experiment, a 2D THz SAR measurement was performed, where the SAR platform was moved in the azimuthal direction (x-axis in Fig. 1). The total number of measurements to achieve the maximal aperture was $N_\xi = 118$, which were performed with a step of $\Delta_\xi = 2$ mm, and the length of emitted frequency ramp was $T = 4.096$ ms. A corner reflector, placed at a reference distance of about $R_0 \approx 1.67$ m, was used as an object under test. Given the reference distance and aperture length 23.4 cm, the integration angle is about $\phi_0 \approx 8.02°$. All the measurement setup parameters are summarized in Table I.

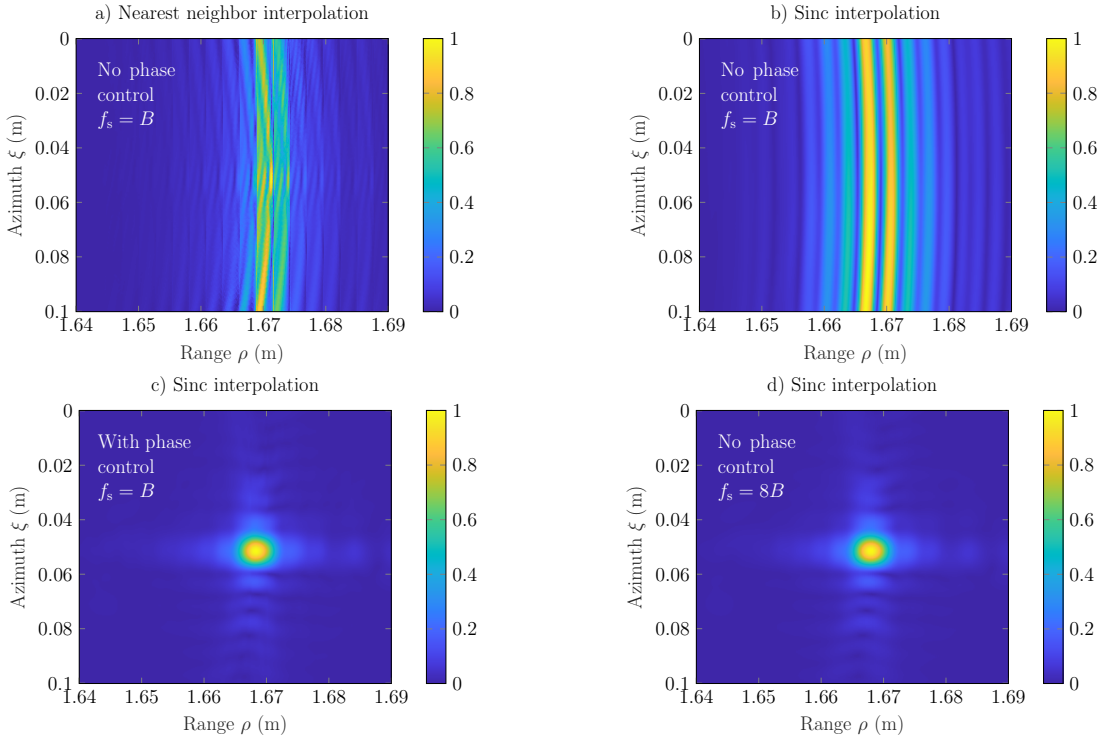

Fig. 2. SAR scenes h of 400×400 pixels reconstructed with nearest neighbor and sinc (for $L = 12$) interpolations: a)–b) and d) without the phase control procedure; c) with the phase-control procedure. In a)–c), the sampling rate $f_s = B = 0.056\,\text{THz}$, and in d), $f_s = 8B = 0.448\,\text{THz}$.

TABLE I
MEASUREMENT SETUP PARAMETERS BASED ON THE FMCW RADAR

Parameter	Value
The lowest frequency processed, $f_{\min}$	0.126 THz
The highest frequency processed, $f_{\max}$	0.182 THz
Ramp duration, T	4.096 ms
Number of range samples, N_ρ	4096
Number of aperture positions, N_ξ	118
Aperture step, Δ_ξ	2 mm
Reference range, R_0	≈ 1.67 m
Integration angle, ϕ_0	$\approx 8.02°$

B. Results

Figure 2 depicts results of SAR scenes h of 400×400 pixels reconstructed via the global backprojection algorithm (9). Here, the intensity of SAR scenes is normalized with corresponding peak intensity values. In Figs. 2a–b, the scenes are obtained based on the nearest neighbor (11) and sinc (12) interpolation algorithms at the sampling rate $f_s = B = 0.056\,\text{THz}$ without the phase control procedure. The response from the corner reflector in these scenes is unfocused, and hence, it can be concluded that these interpolators are not efficient for image reconstruction at the rate $f_s = B$. However, in Fig. 2c is shown the SAR scene reconstruction based on the sinc interpolator (13) with the phase control procedure (14) at the rate $f_s = B$. The results demonstrate that by involving the phase control procedure in the sinc interpolator, it is possible to achieve accurate image reconstruction at the sampling rate $f_s = B$. It should also be noted that the proposed extension (14) is independent of the geometry of targets and their location in the scene under illumination and relies only on rigorous information about the coordinates of the SAR platform antenna and the given point of space in the defined image plane. To achieve image reconstruction results of a similar level via sinc interpolator (12), the sampling rate has to be at least $f_s = B = 0.448\,\text{THz}$, as shown in Fig. 2d.

Figures 3a–b depict range and azimuth SAR-scene cuts $h(\xi, \rho)$ for fixed azimuth $\xi = 0.051\,\text{m}$ and range $\rho = 1.668\,\text{m}$, respectively, where the peak intensity occurs. Here, the SAR-scene functions are obtained based on sinc interpolator (13) with the phase control procedure at sampling rates $f_s \in \{B, 2B\}$ are compared with the functions h based on sinc interpolator (12) without the phase control procedure at the rates $f_s \in \{5B, 6B, 8B\}$. The range and cross-range resolutions are measured in terms of the $-3\,\text{dB}$ beamwidth of the mainlobe from the corresponding cuts; all the measurements are collected in Table II. The results based on (13) for $f_s = B$ and $f_s = 2B$ demonstrate good agreement both in the range and azimuthal cuts in terms of resolution, as indicated in Table II, and the intensity of the first four sidelobes. When the phase control procedure (14) is not included into the sinc interpolator, it has been investigated that the response from the corner reflector can be identified for the sampling rate $f_s \geq 5B$. Furthermore, to achieve agreement with the results

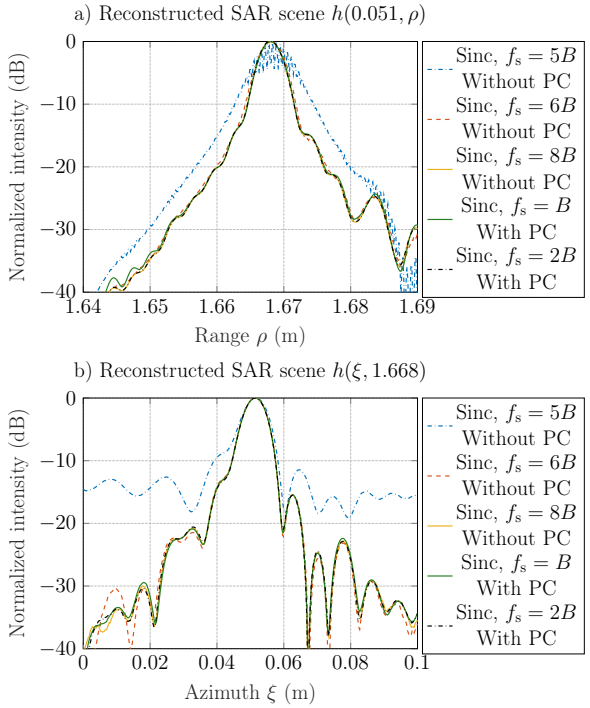

Fig. 3. Evaluation of SAR scene cuts $h(\xi, \rho)$: a) for fixed azimuth $\xi = 0.051$ m; b) for fixed range $\rho = 1.668$ m. Here, the scene cuts are obtained based on sinc interpolation without phase control (PC) at the sampling rates $f_s = 5B = 0.28$ THz, $f_s = 6B = 0.336$ THz, and $f_s = 8B = 0.448$ THz, and with phase control at the rates $f_s = B = 0.056$ THz and $f_s = 2B = 0.112$ THz.

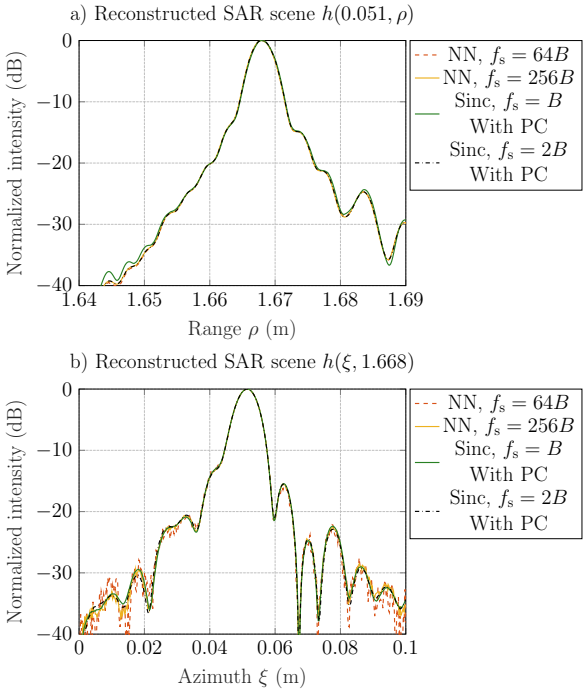

Fig. 4. Evaluation of SAR scene cuts $h(\xi, \rho)$: a) for fixed azimuth $\xi = 0.051$ m; b) for fixed range $\rho = 1.668$ m. Here, the scene cuts are obtained based on nearest neighbor interpolation at the sampling rates $f_s = 64B = 3.584$ THz and $f_s = 256B = 14.336$ THz, and based on sinc interpolation with phase control (PC) at the rates $f_s = B = 0.056$ THz and $f_s = 2B = 0.112$ THz.

obtained based on interpolator (13) in terms of range and cross-range resolutions, the sampling rate has to be $f_s \geq 8B$; see Table II for details. Hence, it can be concluded that an accurate SAR scene reconstruction can be achieved based on sinc interpolator with the phase control procedure at the rate $f_s = B$ and there is no need to perform the FFT-based upsampling procedure to increase the sampling rate f_s.

TABLE II
MEASURED -3 dB RESOLUTION

Interpolation Method	**Axis**	
	Range ρ (mm)	**Azimuth ξ (mm)**
Sinc, $f_s = 5B$, Without PC[1]	5.4	8.1
Sinc, $f_s = 6B$, Without PC	4.1	7.4
Sinc, $f_s = 8B$, Without PC	3.8	7.3
Sinc, $f_s = B$, With PC	3.8	7.3
Sinc, $f_s = 2B$, With PC	3.8	7.3

[1]PC denotes the phase control.

In Figs. 4a–b, the SAR scene cuts $h(\xi, \rho)$, which are obtained based on sinc interpolation with phase control (13) and depicted in Fig. 4, are compared with corresponding range and azimuthal scene cuts obtained based on nearest neighbor interpolator (11) for sampling rates $f_s \in \{64, 256\}$. It has been investigated that to obtain range SAR-scene cuts based on the nearest neighbor interpolator with an accuracy close to the results obtained based on (13), the data has to be sampled at the rate of about $f_s = 20B = 1.12$ THz; however, for azimuthal scene cut, this sampling rate is not sufficient to obtain such a level of accuracy in terms of sidelobe intensity. When the sampling rate is $f_s = 64B$, it is possible to achieve the intensity agreement in the first three sidelobes for azimuthal scene cut; see Fig. 4b. However, to achieve a higher level of accuracy, the sampling rate has to be increased several times higher, to $f_s = 256B$, which is caused by a high sensitivity of the signal's phase to the range-time changes at THz frequencies. Furthermore, for this sampling rate, the computational complexity of the FFT-based upsampling procedure $\mathcal{O}\{2N_\xi u N_\rho \log_2\{uN_\rho\}\}$ will become larger than the computational complexity of the global backprojection algorithm $\mathcal{O}\{N_\xi M_\rho M_\xi\}$. Here, u denotes the upsampling factor, N_ξ and N_ρ are the total numbers of aperture positions and range samples, respectively, and M_ξ and M_ρ are the numbers of SAR scene pixels in azimuthal and range directions, respectively. Hence, the opportunity to avoid the upsampling procedure and to obtain accurate image reconstruction at the sampling rate $f_s = B$ demonstrates the advantages of the proposed sinc interpolation algorithm with the phase control procedure (13) over the conventional nearest neighbor and sinc interpolators.

IV. CONCLUSIONS

In this paper, the extension of the existing sinc interpolation algorithm to process accurately complex-valued SAR data has been proposed. The extension is based on the phase control procedure that assigns information about the range distance between the SAR platform and the point of space in the

defined image plane into the phase of the estimated complex-valued parameter. The proposed extension is independent of the geometry of targets and their location in the scene under illumination and relies only on rigorous information about the coordinates of the SAR platform antenna and the given point of space in the defined image plane. The developed interpolator has been examined on the real data acquired via the FMCW SAR that operates in the range $[0.126, 0.182]$ THz. It has been investigated that by involving the phase control procedure in the sinc interpolator, a SAR scene can be reconstructed at the sampling rate $f_{\mathrm{s}} = B$, which is not achievable based on the conventional nearest neighbor and sinc interpolators. The developed interpolation algorithm can also be incorporated into other backprojection algorithms, such as the fast and the fast-factorized backprojection algorithms.

ACKNOWLEDGMENT

The authors would like to acknowledge 2π-Labs GmbH for providing the radar system for data acquisition.

REFERENCES

[1] A. Batra, M. Wiemeler, D. Goehringer, and T. Kaiser, "Simulation validation of high resolution indoor terahertz synthetic aperture radar imaging," in *2020 14th European Conference on Antennas and Propagation (EuCAP)*. IEEE, 2020, pp. 1–5.

[2] M. Caris, S. Stanko, S. Palm, R. Sommer, A. Wahlen, and N. Pohl, "300 GHz radar for high resolution SAR and ISAR applications," in *2015 16th International Radar Symposium (IRS)*. IEEE, 2015, pp. 577–580.

[3] Y. Zantah, F. Sheikh, A. A. Abbas, M. Alissa, and T. Kaiser, "Channel measurements in lecture room environment at 300 GHz," in *2019 Second International Workshop on Mobile Terahertz Systems (IWMTS)*. IEEE, 2019, pp. 1–5.

[4] A. Batra, V. T. Vu, Y. Zantah, M. Wiemeler, M. I. Pettersson, D. Goehringer, and T. Kaiser, "Sub-mm Resolution Indoor THz Range and SAR Imaging of Concealed Object," in *2020 IEEE MTT-S International Conference on Microwaves for Intelligent Mobility (ICMIM)*. IEEE, 2020, pp. 1–4.

[5] T. Bryllert, K. B. Cooper, R. J. Dengler, N. Llombart, G. Chattopadhyay, E. Schlecht, J. Gill, C. Lee, A. Skalare, I. Mehdi *et al.*, "A 600 GHz imaging radar for concealed objects detection," in *2009 IEEE Radar Conference*. IEEE, 2009, pp. 1–3.

[6] S. Saqueb, N. Nahar, and K. Sertel, "Fast two-dimensional THz imaging using rail-based synthetic aperture radar (SAR) processing," *Electronics Letters*, vol. 56, no. 19, pp. 988–990, 2020.

[7] A. Batra, J. Barowski, D. Damyanov, M. Wiemeler, I. Rolfes, T. Schultze, J. C. Balzer, D. Göhringer, and T. Kaiser, "Short-Range SAR Imaging From GHz to THz Waves," *IEEE Journal of Microwaves*, vol. 1, no. 2, pp. 574–585, 2021.

[8] J. Schorlemer, C. Schulz, N. Pohl, I. Rolfes, and J. Barowski, "Compensation of sensor movements in short-range fmcw synthetic aperture radar algorithms," *IEEE Transactions on Microwave Theory and Techniques*, vol. 69, no. 11, pp. 5145–5159, 2021.

[9] S. Kueppers, T. Jaeschke, N. Pohl, and J. Barowski, "Versatile 126–182 GHz UWB D-band FMCW radar for industrial and scientific applications," *IEEE Sensors Letters*, vol. 6, no. 1, pp. 1–4, 2021.

[10] H. Wang, Y. Zhang, B. Wang, and J. Sun, "A novel helicopter-borne terahertz SAR imaging algorithm based on Keystone transform," in *2014 12th International Conference on Signal Processing (ICSP)*. IEEE, 2014, pp. 1958–1962.

[11] A. Batra, M. El-Absi, M. Wiemeler, D. Göhringer, and T. Kaiser, "Indoor THz SAR trajectory deviations effects and compensation with passive sub-mm localization system," *IEEE Access*, vol. 8, pp. 177 519–177 533, 2020.

[12] L.-E. Andersson, "On the determination of a function from spherical averages," *SIAM Journal on Mathematical Analysis*, vol. 19, no. 1, pp. 214–232, 1988.

[13] A. F. Yegulalp, "Fast backprojection algorithm for synthetic aperture radar," in *Proceedings of the 1999 IEEE Radar Conference. Radar into the Next Millennium (Cat. No. 99CH36249)*. IEEE, 1999, pp. 60–65.

[14] L. M. H. Ulander, H. Hellsten, and G. Stenström, "Synthetic-aperture radar processing using fast factorized backprojection," *IEEE Trans. Aerospace and Electronic Systems*, vol. 39, no. 3, pp. 760–776, 2003.

[15] V. T. Vu and M. I. Pettersson, "Derivation of bistatic SAR resolution equations based on backprojection," *IEEE Geoscience and Remote Sensing Letters*, vol. 15, no. 5, pp. 694–698, 2018.

[16] R. Hanssen and R. Bamler, "Evaluation of interpolation kernels for SAR interferometry," *IEEE Transactions on Geoscience and Remote Sensing*, vol. 37, no. 1, pp. 318–321, 1999.

[17] Z. Li and J. Bethel, "Image coregistration in SAR interferometry," *The International Archives of the Photogrammetry, Remote Sensing and Spatial Information Sciences*, vol. 37, pp. 433–438, 2008.

[18] Y. Ivanenko, V. T. Vu, and M. I. Pettersson, "Interpolation methods for SAR backprojection at THz frequencies," in *2021 Fourth International Workshop on Mobile Terahertz Systems (IWMTS)*. IEEE, 2021, pp. 1–5.

[19] J. G. Proakis and D. G. Manolakis, *Digital Signal Processing*, 4th ed. Pearson Education, Inc., 2007.